Near-Wall Turbulence Closure for Curved Flows

R. M. C. So* and Y. G. Lai†
Arizona State University, Tempe, Arizona 85287
and
B. C. Hwang‡
David Taylor Research Center, Annapolis, Maryland 21402

At present, turbulence closures for curved flows only account for curvature effects in the fully turbulent region where the Reynolds number is large. The justification is that, near a wall, viscous effects dominate and curvature effects are only of secondary importance. Recent direct simulation data show that this assumption is not valid, even for simple two-dimensional fully developed turbulent curved channel flows. This paper presents an approach to develop a near-wall turbulence closure for wall-bounded curved flows. The curved channel direct simulation data is used as a guide to help develop such a closure. The proposed closure has the unique property of approaching conventional high-Reynolds-number Reynolds-stress closures far away from the wall. Hence, curvature effects in both the near-wall and the fully turbulent parts of the flow are accounted for properly. Validations of the closure are carried out with a set of low-Reynolds-number simulation data and with experimental measurements at high Reynolds number. Good agreement is obtained in both cases; in particular, the anisotropic behavior of the normal stresses and the shear stress behavior near the convex and concave walls.

I. Introduction

MODELING of wall-bounded curved shear flows can be broadly classified into three different types. The first, which is also the simplest, is based on a modification of either the mixing length or the eddy viscosity by a curvature parameter[1-6] labeled by Bradshaw[1] as an F factor correction. This F factor can be derived from the Reynolds-stress transport equations through the assumption of equilibrium turbulence[2-5] or by invoking a semi-equilibrium turbulence assumption.[6] The F factors thus derived are nonlinear in terms of the curvature parameter. However, if the curvature parameter is assumed to be small and equilibrium turbulence is invoked, all of the F factors can be shown to reduce to the linear form proposed by Bradshaw.[1] As such, the corrections are applicable only in the region far away from the wall, where the flow is dominated by fully turbulent flow and is independent of Reynolds number. The flow very close to the wall is either handled by incorporating viscous damping to model near-wall viscosity effects[2-4,6] or by invoking wall function approximations.[5] These approaches are justified by arguing that curvature effects are of secondary importance in a highly viscous flow.[1]

The second type consists of closures that solve modified transport equations of characteristic velocity and length scales. This type of closure differs from the first in that there is no F factor applied to the mixing length or eddy viscosity. Rather, the transport equations that govern the velocity and length scales that are used to form the eddy viscosity are modified to include curvature effects. For example, the equations that govern the transport of the dissipation rate of turbulent kinetic energy and the variance of the normal fluctuating velocity are modified to include extra production terms due to streamline curvature.[7] Even though the equations solved are applicable all the way to the wall, the effects of curvature on the near-wall turbulence field have not been accounted for properly.

The third type is the most general of the three different types of closure. It is based on the modeled Reynolds-stress transport equations,[8,9] and is intended as an improvement over the first two types. The improvements come in three major areas. First and foremost is the relaxation of the gradient-transport assumption. This means that the turbulent shear stress is calculated directly by solving its own transport equation simultaneously with other governing equations. The second improvement is the relaxation of the equilibrium and semi-equilibrium assumption. By doing so, the closure is more applicable to shear flows with large streamline curvature. It has been observed that strong stabilizing curvature could result in a "cut-off" of turbulent shear and subsequent creation of regions of small negative energy production far away from the wall.[10] Therefore, it is not easily justified to neglect transport effects on the turbulence field. The third improvement is in the closures' ability to predict the anisotropy of the normal stresses, depending on the modeling of the various terms in the Reynolds-stress transport equation. Thus, the closure provides the added freedom to model the Reynolds-stress equation in such a way that the suppression of turbulence by strong stabilizing curvature could be accounted for properly. Indeed, this type of closure gives better agreement with measurements[8,9] over a wider range of curvature parameter compared to the first two types. However, it also suffers from the drawback of wall-function assumptions. The reason is that the modeled terms in the Reynolds-stress equation are, strictly speaking, valid for high-Reynolds-number flows, and are not applicable to the flow very near a wall.

The inadequacies of the different types of closure are plainly evident by their performance when applied to calculate relatively simple curved flows in the 1980-1981 AFOSR-HTTM-Stanford Conference on complex turbulent flows.[11] According to Bradshaw,[12] one difficulty is the surprisingly large effect exerted on the turbulence field by streamline curvature in the plane of the mean shear. Often this effect is one order of magnitude larger than that predicted by dimensional arguments. This lack of understanding of curvature effects hinders the development of more appropriate closures for curved shear flows.

Recently, the effects of curvature on turbulent wall shear flows were studied by direct simulation of the Navier-Stokes equations at a fairly low Reynolds number.[13] Among the findings is the similarity of many of the turbulence statistics of

Received Feb. 28, 1990; revision received June 4, 1990; accepted for publication June 5, 1990.

*Professor, Mechanical and Aerospace Engineering.
†Graduate Assistant, Mechanical and Aerospace Engineering.
‡Research Scientist.

interest on the concave and convex side of a curved channel when properly scaled using local wall variables. The exceptions to the similarity are the Reynolds shear stress and the terms governing the balance of the Reynolds shear stress equation. This means that streamline curvature has its greatest effect on the Reynolds shear stress equation and suggests that curvature effects should be modeled in a Reynolds-stress closure rather than in a $k-\epsilon$ type closure. Furthermore, the direct simulation results show that it is important to model the pressure-strain term correctly, particularly near a wall, to account for curvature effects.

The objective of the present study is to make use of the direct simulation data on curved channel flow[13] to devise a Reynolds-stress closure for curved shear flows. Since the study of Moser and Moin[13] points out the significance of the similarity of the turbulence statistics on the concave and convex walls when scaled with local variables, it is important to devise a near-wall closure for curved flows rather than continuing to rely on wall-function approximations. These approximations are not appropriate for curved flows because they are based on one set of wall variables, while in a curved channel flow, the wall variables on the concave side differ from those on the convex side. Therefore, the present approach to formulate a near-wall Reynolds-stress closure is to attempt to model curvature effects in both the near-wall and fully turbulent regions of the wall-bounded curved flows. Obviously, far away from the wall, the performance of the proposed closure has to approximate closely that of established models, such as Irwin and Arnot Smith,[8] Gibson et al.,[9] and Launder et al.[14]

II. Near-Wall Behavior of Curved Flows

Unlike plane flows, where detailed near-wall measurements of the Reynolds stresses are available, there are practically no measurements available for curved flows. Therefore, an analysis of the near-wall behavior of curved flows has to rely solely on the direct simulation data generated on a fully developed turbulent flow in a two-dimensional curved channel.[13] The simulation was carried out with a curvature parameter of $h/r_c = 1/79$, where h is the channel halfwidth and r_c is the mean radius of curvature, and a Reynolds number based on h and channel centerline velocity of 2990. Moser and Moin[13] defined a global friction velocity u_τ based on the mean pressure gradient $(1/r)\,(d\bar{P}/d\theta)$, so that

$$u_\tau = \left(-\frac{1}{r_c\rho}\frac{d\bar{P}}{d\theta}\right)^{1/2} = \left(\frac{r_i^2 u_{\tau i}^2 + r_o^2 u_{\tau o}^2}{2r_c^2}\right)^{1/2} \tag{1}$$

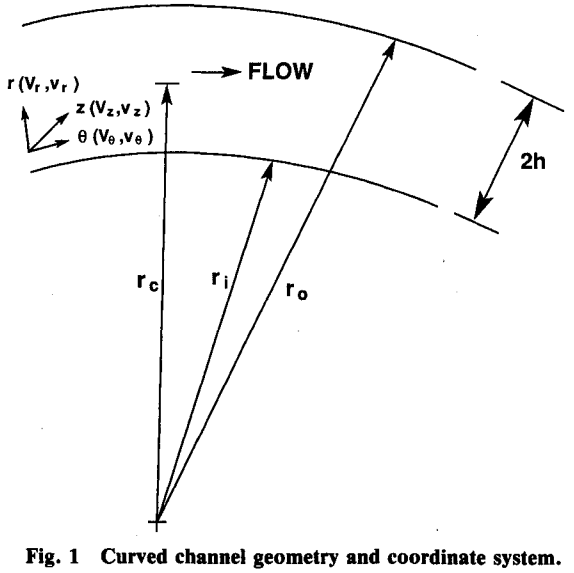

Fig. 1 Curved channel geometry and coordinate system.

where r_i and r_o are the inner (convex) and outer (concave) radius of the channel, $u_{\tau i}$ and $u_{\tau o}$ the inner and outer wall friction velocity, and ρ is fluid density. The corresponding Reynolds number based on h and the three different friction velocities are $Re = 168$, $Re_i = 155$, and $Re_o = 180$.

When the mean velocity and the turbulent normal stresses are made dimensionless using local wall variables and plotted against log x_2^+ (where $x_2^+ = u_{\tau i}x_2/\nu$ or $u_{\tau o}\,x_2/\nu$ and x_2 is the coordinate measured normal to the wall) for the mean velocities and against x_2^+ for the normal stresses, the results show that there is essentially no difference between the flow properties near concave and convex walls for $x_2^+ < 20$. Furthermore, the direct simulation data near a wall is in good agreement with plane channel flow measurements[15] and plane channel simulation data.[16,17] On the other hand, the turbulent shear stress near the concave and convex walls starts to deviate from each other beginning around $x_2^+ = 15$, with the turbulent shear stress on the side of the concave wall higher than that of the plane channel data and lower on the convex side. Furthermore, the direct simulation data reveals that the 22 components of pressure diffusion in the near-wall region is comparable in magnitude to pressure strain, but the 11, 33, and 12 components of pressure diffusion are small in the near-wall region. These results suggest that near a wall, whether plane, convex, or concave, the 22 components of pressure diffusion acts to decrease the fluctuating velocity normal to the wall and in turn the other components. Therefore, the mean and fluctuating velocity components, U_i and u_i, could be expanded in terms of the normal coordinate x_2; thus,

$$U_i = A_i x_2 + B_i x_2^2 + C_i x_2^3 + \ldots \tag{2a}$$

$$u_i = a_i x_2 + b_i x_2^2 + c_i x_2^3 + \ldots \tag{2b}$$

where A_i, B_i, C_i are constants or functions of x_1 and x_3 and a_i, b_i, c_i are random functions of time and x_1 and x_3, the stream and transverse coordinates. For incompressible flows, continuity requires that $A_2 \equiv 0$ and $a_2 \equiv 0$.

The present approach is to use Eq. (2) to analyze the near-wall behavior of the various terms in the Reynolds-stress equation. This knowledge is then applied to model the terms in the Reynolds-stress equations so that the near-wall behavior of the exact as well as the modeled equation is similar, at least to the lowest order of x_2 for each term. Thus, the near-wall balance of the modeled Reynolds-stress equation is assured and the possibility of success of the proposed near-wall closure is enhanced.

III. Near-Wall Turbulence Closure

The Reynolds-stress equation for incompressible flows can be symbolically written as[14,18]

$$C_{ij} = D_{ij}^{\nu} + D_{ij}^{T} + P_{ij} + \Phi_{ij}^{*} - \epsilon_{ij} \tag{3}$$

where C_{ij} is the convection of $\overline{u_i u_j}$, D_{ij}^{ν} and D_{ij}^{T} are the viscous and turbulent diffusion of $\overline{u_i u_j}$, P_{ij} is the production of $\overline{u_i u_j}$ by mean shear, Φ_{ij}^{*} is the velocity pressure-gradient correlation, and ϵ_{ij} is the viscous dissipation of $\overline{u_i u_j}$. With the exception of Φ_{ij}^{*}, the near-wall behavior of all of the terms in Eq. (3) can be analyzed using Eq. (2). As suggested by Lai and So,[19] however, Eq. (3) can be used to obtain the near-wall behavior of Φ_{ij}^{*}. They carried out this analysis and found that, near a wall, the behavior of Φ_{ij}^{*}, at least to $\mathcal{O}(x_2^2)$ is governed by the term $(D_{ij}^{\nu} - \epsilon_{ij})$. The lowest-order term for C_{ij}, D_{ij}^{T}, and P_{ij} is $\mathcal{O}(x_2^3)$. Therefore, these terms are not of primary importance in determining the near-wall behavior of Eq. (3). Among the various terms in Eq. (3), D_{ij}^{T}, Φ_{ij}^{*}, and ϵ_{ij} need modeling. The earlier analysis shows that, to $\mathcal{O}(x_2^2)$, near-wall modeling of D_{ij}^{T} is not necessary; however, it is of paramount importance to Φ_{ij}^{*} and ϵ_{ij}.

Two different approaches can be used to devise models for D_{ij}^{T}, Φ_{ij}^{*}, and ϵ_{ij}. One approach is to start from scratch, while

the second is to build on the proven high-Reynolds-number models. Since D_{ij}^T is not important in the near-wall region, the high-Reynolds-number models of Refs. 9 and 18 can be assumed. These are proven models for D_{ij}^T and, therefore, suggest that the second approach would be a more fruitful first attempt to formulate a near-wall Reynolds-stress closure. In other words, the high-Reynolds-number models for Φ_{ij}^* and ϵ_{ij} should be modified to account for wall effects so that the modeled form of Eq. (3) remains in balance as the wall is approached.

The commonly used high-Reynolds-number model for ϵ_{ij} is the isotropic model of Kolmogorov.[20] However, the model does not satisfy the near-wall kinematic conditions for $\epsilon_{ij}/\overline{u_iu_j}$ as discussed by Launder and Reynolds.[21] Furthermore, it fails to asymptote correctly to the boundary condition for ϵ_{ij}. Using the proposal of Ref. 21 as a guide, Lai and So[19] derived a modified model for ϵ_{ij} that satisfies the kinematic condition for $\epsilon_{ij}/\overline{u_iu_j}$ as well as the boundary condition for ϵ_{ij}. Their model is given by

$$\epsilon_{ij} = (2/3)\epsilon(1-f_{w,1})\delta_{ij} + f_{w,1}(\epsilon/k)\left[\overline{u_iu_j} + \overline{u_iu_k}n_kn_j + \overline{u_ju_k}n_kn_i + n_iu_j\overline{u_ku_l}n_kn_l\right]\Big/\left[1+3\overline{u_ku_l}n_kn_l/2k\right] \quad (4)$$

where $f_{w,1} = \exp[-(R_T/150)^2]$, $R_T = k^2/\nu\epsilon$, k is the turbulent kinetic energy and ϵ its dissipation rate, ν is the fluid kinematic viscosity, and $n_i = (0,1,0)$ is the unit normal vector measured positive away from the wall. It can be seen that ϵ_{ij} contracts correctly to 2ϵ just like the isotropic model. In addition, $f_{w,1}$ goes to zero exponentially away from the wall, so that the isotropic model of Kolmogorov is recovered in the limit as R_T becomes very large.

Conventional high-Reynolds-number modeling of Φ_{ij}^* is to partition the term into Φ_{ij}^p, the pressure-diffusion part which is neglected, and Φ_{ij}, the pressure-strain part that is retained. This treatment is quite successful for high-Reynolds-number flows. But it has two drawbacks. One is that a second-order tensor with a zero trace is used to represent Φ_{ij}^*, which has a nonzero trace. Another is more serious. All components of Φ_{ij}^* go to zero at the wall, while the same is not true for Φ_{ij}. Essentially, it is this partition of Φ_{ij}^* that renders the Reynolds-stress equation not valid near the wall. In order to build on the high-Reynolds-number models for Φ_{ij}, the modifications made to Φ_{ij} have to render the modeled terms of Φ_{ij}^* satisfy the wall boundary condition as well as the near-wall balance given by $(D_{ij}^v - \epsilon_{ij})$ as discussed earlier. Therefore, it can be seen that the modifications are dependent on the high-Reynolds-number models assumed for Φ_{ij} and are proposed to counter the incorrect behavior of Φ_{ij} near a wall as well as to partially model the neglect of the term Φ_{ij}^p. Based on the discussions of Moser and Moin[13] and Lai and So,[19] it seems that the pressure-strain model of Launder et al.[14] is most appropriate for Φ_{ij}. Therefore, the present approach adopts Launder et al.'s[14] model for Φ_{ij} and proceeds to modify the Φ_{ij} so that the resultant model for Φ_{ij}^* satisfies the conditions discussed earlier. Along the procedure outlined earlier, Lai and So[19] proposed to model Φ_{ij}^* as

$$\Phi_{ij}^* = \Phi_{ij} + f_{w,1}\left[C_1\frac{\epsilon}{k}\left(\overline{u_iu_j} - \frac{2}{3}k\delta_{ij}\right) - \frac{\epsilon}{k}\left(\overline{u_iu_k}n_kn_j + \overline{u_ju_k}n_kn_i\right) + \alpha^*\left(P_{ij} - \frac{2}{3}\tilde{P}\delta_{ij}\right)\right] \quad (5)$$

where

$$\Phi_{ij} = -C_1\frac{\epsilon}{k}\left(\overline{u_iu_j} - \frac{2}{3}k\delta_{ij}\right) - \alpha\left(P_{ij} - \frac{2}{3}\tilde{P}\delta_{ij}\right) - \beta\left(D_{ij} - \frac{2}{3}\tilde{P}\delta_{ij}\right) - \gamma k\left(\frac{\partial U_i}{\partial x_j} + \frac{\partial U_j}{\partial x_i}\right)$$

$$D_{ij} = -\left[\overline{u_iu_k}\frac{\partial U_k}{\partial x_j} + \overline{u_ju_k}\frac{\partial U_k}{\partial x_i}\right]$$

$\tilde{P} = P_{ii}/2$, $\alpha = (8+C_2)/11$, $\beta = (8C_1-2)/11$, $\gamma = (30C_2-2)/55$, C_1 and C_2 are model constants introduced by Launder et al.,[14] and α^* is a new model constant. This model compensates the

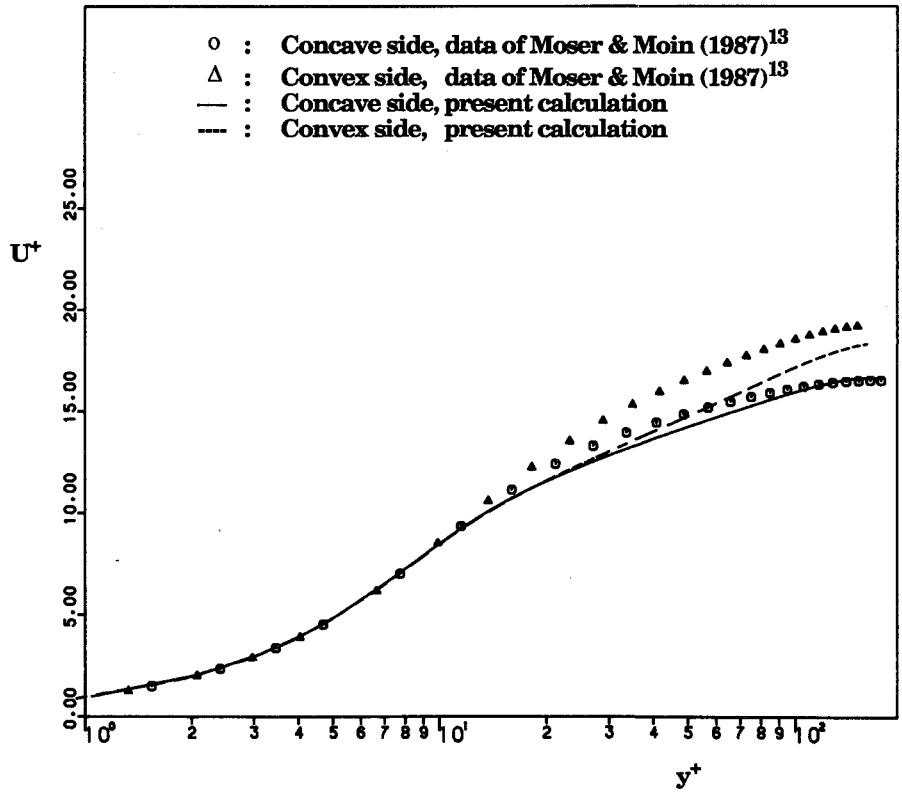

Fig. 2 Mean velocities in wall coordinates.

incorrect near-wall behavior of Φ_{ij} and, at the same time, provides a pressure diffusion component in the x_2 direction. This model was found to give excellent prediction for the near-wall anisotropy of the turbulent normal stresses.[19] Therefore, it is adopted for Φ_{ij}^* in the present approach.

The near-wall modeling of Eq. (3) is then completed by specifying a model for D_{ij}^T. Since it is not necessary to model D_{ij}^T near a wall, at least to $\mathcal{O}(x_2^2)$, the proposal is to adopt the high-Reynolds-number model of Hanjalic and Launder.[18] This model has two advantages. One is that the model is tensorially correct for the term $-\overline{u_i u_j u_k}$ to be modeled. Another is the anisotropic diffusion property of the model. Therefore, D_{ij}^T can be written as

$$D_{ij}^T = \frac{\partial}{\partial x_k}\left[C_s \frac{k}{\epsilon}\left\{\overline{u_i u_l}\frac{\partial \overline{u_j u_k}}{\partial x_l} + \overline{u_j u_l}\frac{\partial \overline{u_k u_i}}{\partial x_l} + \overline{u_k u_l}\frac{\partial \overline{u_i u_j}}{\partial x_l}\right\}\right] \quad (6)$$

where C_s is a model constant.

IV. Near-Wall ϵ-Equation

The model Eqs. (4–6) introduce yet another unknown ϵ into the formulation. To effect closure, either ϵ is prescribed, or another equation governing its transport has to be solved. The proposed ϵ equation has to be valid as a wall is approached. Otherwise, the near-wall balance of the modeled Eq. (3) will be destroyed and the near-wall Reynolds-stress closure will no longer be valid near a wall. Lai and So[19] have analyzed the ϵ equation of Shima[22] and have proposed modifications to make the resultant equation comply with all of the near-wall conditions discussed earlier. Their proposal is

$$\frac{D\epsilon}{Dt} = \frac{\partial}{\partial x_k}\left(\nu \frac{\partial \epsilon}{\partial x_k}\right) + \frac{\partial}{\partial x_k}\left(C_\epsilon \frac{k}{\epsilon}\overline{u_k u_i}\frac{\partial \epsilon}{\partial x_i}\right)$$

$$+ C_{\epsilon 1}(1 + \sigma f_{w,2})\frac{\epsilon}{k}\tilde{P} - C_{\epsilon 2} f_\epsilon \frac{\epsilon\tilde{\epsilon}}{k} + \xi \quad (7)$$

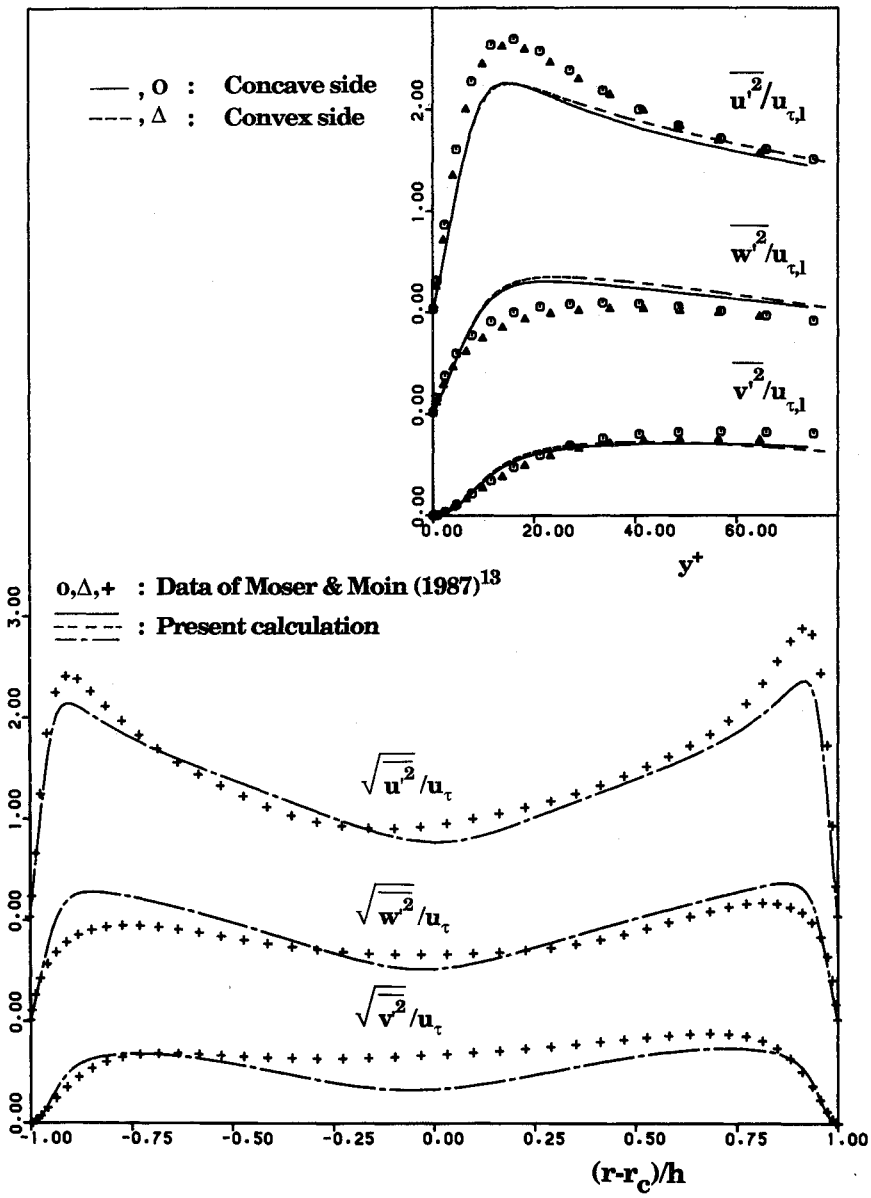

Fig. 3 Distributions of the normal stresses.

where

$$\xi = f_{w,2}\left[\left(\frac{7}{9}C_{\epsilon 2}-2\right)\frac{\epsilon\tilde{\epsilon}}{k}-\frac{\epsilon^{*2}}{2k}\right]$$

$$f_{w,2} = \exp\left[-\left(\frac{R_T}{64}\right)^2\right]$$

$$f_\epsilon = 1-\frac{2}{9}\exp\left[-\left(\frac{R_T}{6}\right)^2\right]$$

$$\sigma = 1-0.6\exp\left[-\frac{R_D}{10^4}\right]$$

$$\tilde{\epsilon} = \epsilon - 2\nu\left(\frac{\partial\sqrt{k}}{\partial x_2}\right)^2, \qquad \epsilon^* = \epsilon - \frac{2\nu k}{x_2^2}$$

R_D is the Reynolds number based on channel halfwidth and mean centerline velocity, and C_ϵ, $C_{\epsilon 1}$, and $C_{\epsilon 2}$ are model constants. Unlike the boundary conditions for $\overline{u_i u_j}$, which are zero at the wall, the wall boundary condition for ϵ is $2\nu(\partial\sqrt{k}/\partial x_2)^2$, because this is the correct ϵ behavior at the wall. It should be pointed out that σ renders the ϵ equation Reynolds-number dependent and is a direct consequence of Mansour et al.'s analysis[23] of the plane channel flow simulation data.[16,17] σ is essentially equal to one for high-Reynolds-number flows. However, the general nature of σ still remains to be verified.

V. Governing Equations for Curved Channel Flows

Validations of the turbulence closure should be carried out with little or no influence from numerical errors. Since the governing equations for fully developed turbulent flows can be reduced to ordinary differential equations and, therefore, can be solved by any known numerical technique with a minimum of numerical errors, it would seem prudent to first attempt to validate the near-wall turbulence closure by considering fully developed curved channel flows.

Incompressible, fully developed turbulent flow through a curved channel is considered. The aspect ratio of the channel is assumed to be large, so that the secondary motion is confined to the end walls and the flow in the channel midplane is essentially two dimensional. A cylindrical coordinate system (r,θ,z) is used to describe the flow (Fig. 1). The mean and fluctuating velocities are given by $(0,U_\theta,0)$ and (u_r,u_θ,u_z) respectively. The governing equations for this flow can be written in dimensionless form by normalizing U_θ by the global

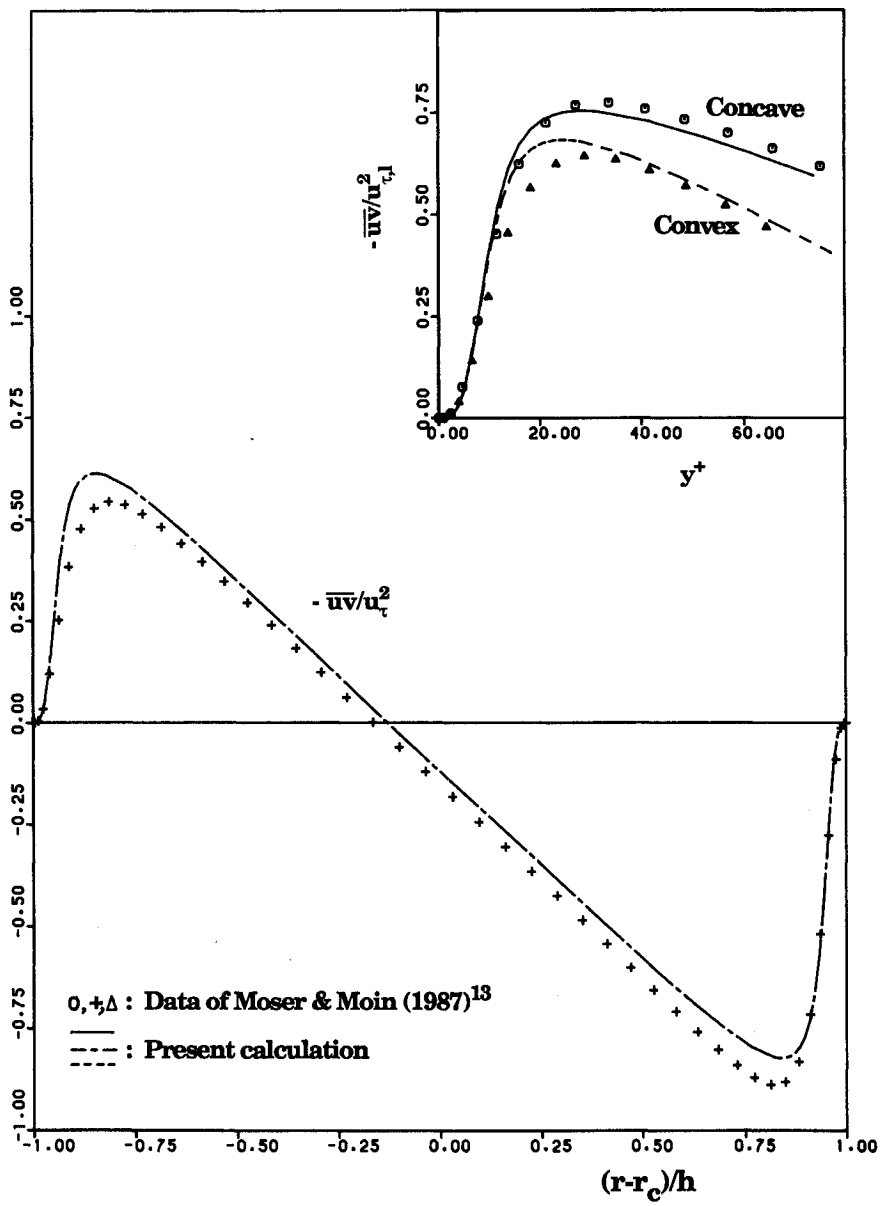

Fig. 4 Shear stress distribution across curved channel.

friction velocity u_τ, $\overline{u_i u_j}$ by u_τ^2, ϵ by u_τ^4/ν, and the r coordinate in such a way that $\eta^+ = (r - r_c)\, u_\tau/\nu$. If the continuity equation and the conditions $\partial(\,)/\partial\theta = \partial(\,)/\partial z = 0$ are used to simplify the mean flow, the Reynolds stress and the ϵ equations, the resultant equations, written with $(0, U^+, 0)$ and (v, u, w) to denote the dimensionless velocity components and ϵ to denote the dimensionless dissipation rate, are

$$\frac{1}{\eta^+ + \delta Re}\frac{\mathrm{d}}{\mathrm{d}\eta^+}\left[(\eta^+ + \delta Re)\frac{\mathrm{d}U^+}{\mathrm{d}\eta^+}\right] - \frac{1}{\eta^+ + \delta Re} \times \frac{\mathrm{d}}{\mathrm{d}\eta^+}\left[(\eta^+ + \delta Re)\overline{uv}\right] - \frac{\overline{uv}}{\eta^+ + \delta Re} - \frac{U^+}{(\eta^+ + \delta Re)^2} + \frac{\delta}{\eta^+ + \delta Re} = 0 \tag{8}$$

$$\frac{1}{\eta^+ + \delta Re}\frac{\mathrm{d}}{\mathrm{d}\eta^+}\left[(\eta^+ + \delta Re)\left(1 + C_s\frac{k}{\epsilon}\overline{v^2}\right)\frac{\mathrm{d}\overline{u^2}}{\mathrm{d}\eta^+}\right] + \frac{2}{\eta^+ + \delta Re}\frac{\mathrm{d}}{\mathrm{d}\eta^+}\left[(\eta^+ + \delta Re)C_s\frac{k}{\epsilon}\overline{uv}\frac{\mathrm{d}\overline{u^2}}{\mathrm{d}\eta^+}\right] + \frac{2}{\eta^+ + \delta Re}\frac{\mathrm{d}}{\mathrm{d}\eta^+}\left[C_s\frac{k}{\epsilon}\left\{(\overline{uv})^2 + \overline{u^2}(\overline{v^2} - \overline{u^2})\right\}\right] + \frac{4}{\eta^+ + \delta Re}\left[C_s\frac{k}{\epsilon}\overline{uv}\frac{\mathrm{d}\overline{uv}}{\mathrm{d}\eta^+} + C_s\frac{k}{\epsilon}\overline{uv}\frac{\overline{uv}}{\eta^+ \delta Re} + C_s\frac{k}{\epsilon}\overline{u^2}\frac{\overline{v^2} - \overline{u^2}}{\eta^+ + \delta Re}\right] + \frac{2}{\eta^+ + \delta Re}C_s\frac{k}{\epsilon}\overline{v^2}\frac{\mathrm{d}\overline{u^2}}{\mathrm{d}\eta^+} + \frac{2(\overline{v^2} - \overline{u^2})}{(\eta^+ + \delta Rc)^2} - C_1(1 - f_{w,1})\frac{\epsilon}{k}\left(\overline{u^2} - \frac{2}{3}k\right) - 2\overline{uv}\frac{\mathrm{d}U^+}{\mathrm{d}\eta^+} - 2\overline{uv}\frac{U^+}{\eta^+ + \delta Re} + \frac{2}{3}(\alpha - \alpha^* f_{w,1}) \times \left[2\overline{uv}\frac{\mathrm{d}U^+}{\mathrm{d}\eta^+} + \overline{uv}\frac{U^+}{\eta^+ + \delta Re}\right] - \frac{2}{3}\beta\left[2\overline{uv}\frac{U^+}{\eta^+ + \delta Re} + \overline{uv}\frac{\mathrm{d}U^+}{\mathrm{d}\eta^+}\right] - \frac{2}{3}\epsilon(1 - f_{w,1}) - f_{w,1}\frac{(\epsilon/k)\overline{u^2}}{1 + 3\overline{v^2}/2k} = 0 \tag{9}$$

$$\frac{1}{\eta^+ \delta Re}\frac{\mathrm{d}}{\mathrm{d}\eta^+}\left[(\eta^+ + \delta Re)\left(1 + 3C_s\frac{k}{\epsilon}\overline{v^2}\right)\frac{\mathrm{d}\overline{v^2}}{\mathrm{d}\eta^+}\right] - \frac{3}{\eta^+ + \delta Re}\frac{\mathrm{d}}{\mathrm{d}\eta^+}\left[2C_s\frac{k}{\epsilon}(\overline{uv})(\overline{uv})\right] - \frac{2}{\eta^+ + \delta Re}C_s\frac{k}{\epsilon} \times \left[\overline{v^2}\frac{\mathrm{d}\overline{u^2}}{\mathrm{d}\eta^+} + 2\overline{uv}\frac{\mathrm{d}\overline{uv}}{\mathrm{d}\eta^+} + 2\overline{uv}\frac{\overline{uv}}{\eta^+ + \delta Re} + 2\overline{u^2}\frac{\overline{v^2} - \overline{u^2}}{\eta^+ + \delta Re}\right] + \frac{2(\overline{u^2} - \overline{v^2})}{(\eta^+ + \delta Re)^2} + 4\overline{uv}\frac{U^+}{\eta^+ + \delta Re} - C_1(1 - f_{w,1})\frac{\epsilon}{k} \times \left(\overline{v^2} - \frac{2}{3}k\right) - \frac{2}{3}(\alpha - \alpha^* f_{w,1})\left[2\overline{uv}\frac{U^+}{\eta^+ + \delta Re} + \overline{uv}\frac{\mathrm{d}U^+}{\mathrm{d}\eta^+}\right] + \frac{2}{3}\beta\left[2\overline{uv}\frac{\mathrm{d}U^+}{\mathrm{d}\eta^+} + \overline{uv}\frac{U^+}{\eta^+ + \delta Re}\right] - 2f_{w,1}\frac{\epsilon}{k}\overline{v^2} - \frac{2}{3}\epsilon(1 - f_{w,1}) - 4f_{w,1}\frac{(\epsilon/k)\overline{v^2}}{1 + 3\overline{v^2}/2k} = 0 \tag{10}$$

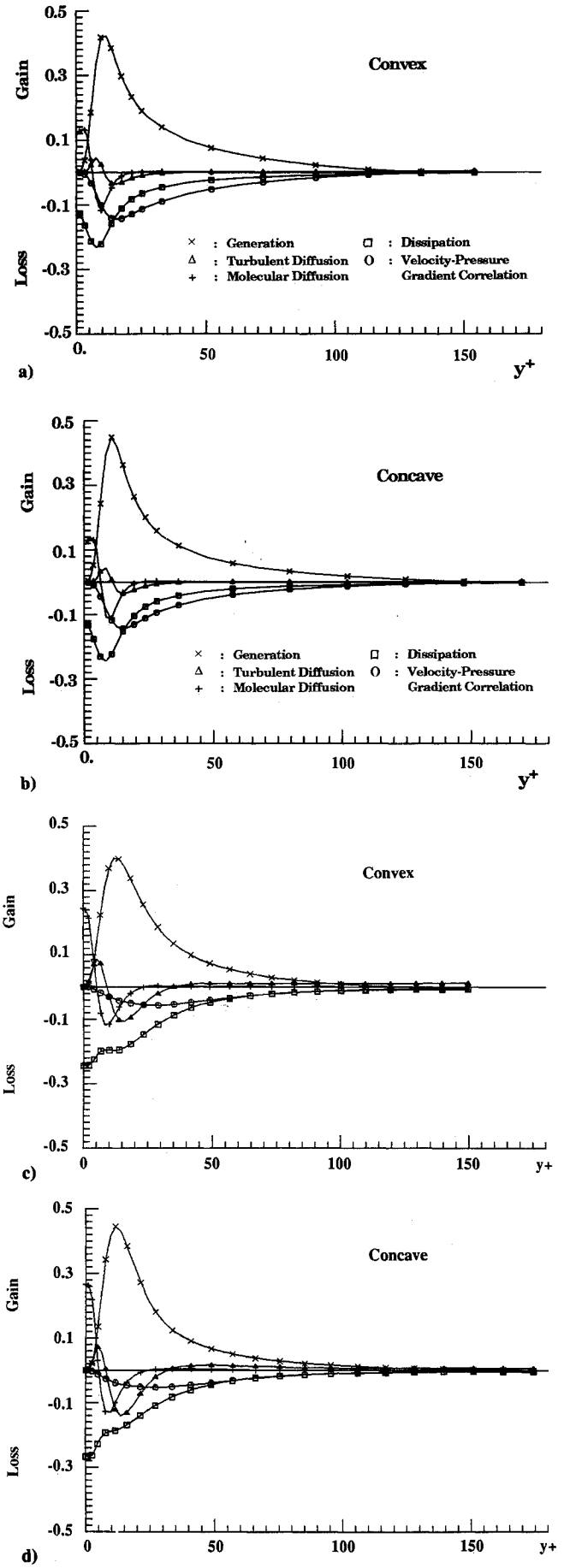

Fig. 5 Budgets of $\overline{u^2}$ in the near-wall region. Model calculations: a) convex wall, and b) concave wall. Direct simulation: c) convex wall, and d) concave wall.

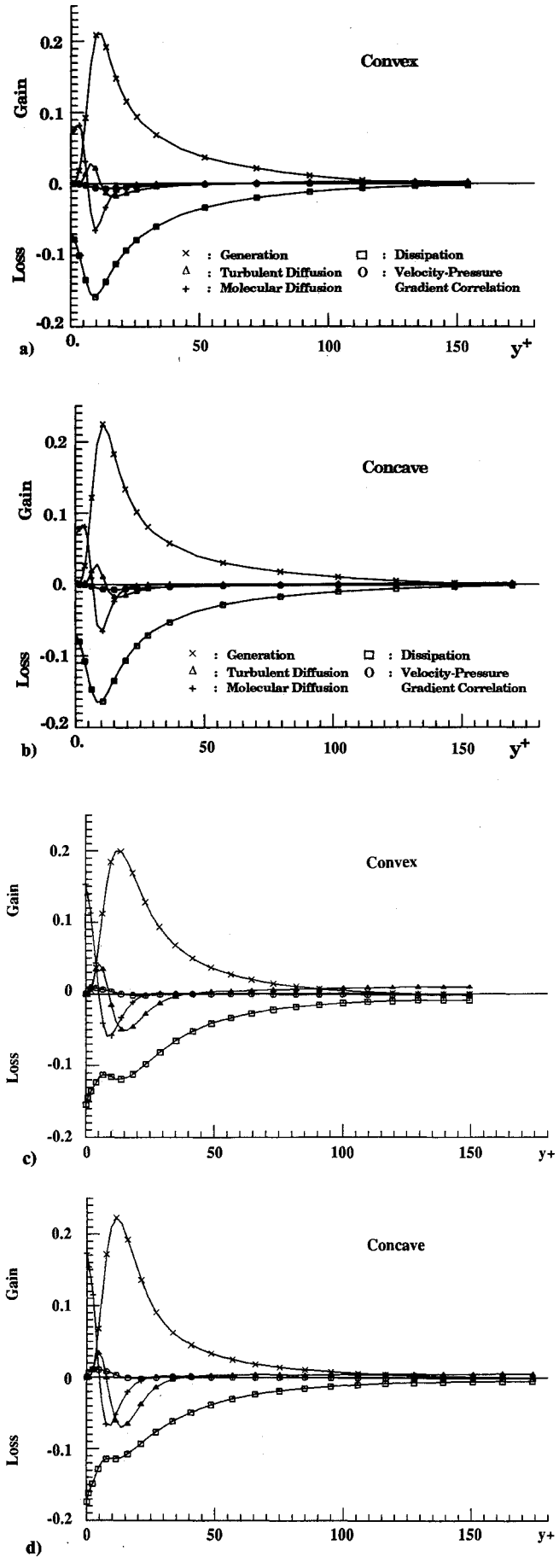

Fig. 6 Budgets of k in the near-wall region. Model calculations: a) convex wall, and b) concave wall. Direct simulation: c) convex wall, and d) concave wall.

$$\frac{1}{\eta^+ + \delta Re}\frac{\mathrm{d}}{\mathrm{d}\eta^+}\left[(\eta^+ + \delta Re)\left(1 + C_s\frac{k}{\epsilon}\overline{v^2}\right)\frac{\mathrm{d}\overline{w^2}}{\mathrm{d}\eta^+}\right]$$
$$- C_1(1 - f_{w,1})\frac{\epsilon}{k}\left(\overline{w^2} - \frac{2}{3}k\right) - \frac{2}{3}(\alpha - \alpha^* f_{w,1})$$
$$\times\left[uv\frac{\mathrm{d}U^+}{\mathrm{d}\eta^+} - uv\frac{U^+}{\eta^+ + \delta Re}\right]$$
$$- \frac{2}{3}\beta\left[\overline{uv}\frac{\mathrm{d}U^+}{\mathrm{d}\eta^+} - \overline{uv}\frac{U^+}{\eta^+ + \delta Re}\right]$$
$$- \frac{2}{3}\epsilon(1 - f_{w,1}) - f_{w,1}\frac{(\epsilon/k)\,\overline{w^2}}{1 + 3\overline{v^2}/2k} = 0 \tag{11}$$

$$\frac{1}{\eta^+ + \delta Re}\frac{\mathrm{d}}{\mathrm{d}\eta^+}\left[(\eta^+ + \delta Re)\left(1 + 2C_s\frac{k}{\epsilon}\overline{v^2}\right)\frac{\mathrm{d}\overline{uv}}{\mathrm{d}\eta^+}\right]$$
$$+ \frac{1}{\eta^+ + \delta Re}\frac{\mathrm{d}}{\mathrm{d}\eta^+}\left[(\eta^+ + \delta Re)C_s\frac{k}{\epsilon}\overline{uv}\frac{\mathrm{d}\overline{v^2}}{\mathrm{d}\eta^+}\right]$$
$$+ \frac{2}{\eta^+ + \delta Re}\frac{\mathrm{d}}{\mathrm{d}\eta^+}\left[(\eta^+ + \delta Re)C_s\frac{k}{\epsilon}\overline{uv}\frac{\overline{v^2} - 2\overline{u^2}}{\eta^+ + \delta Re}\right]$$
$$+ \frac{1}{\eta^+ + \delta Re}C_s\frac{k}{\epsilon}\left[2\overline{v^2}\frac{\mathrm{d}\overline{uv}}{\mathrm{d}\eta^+} + \overline{uv}\frac{\mathrm{d}\overline{v^2}}{\mathrm{d}\eta^+} + 2\overline{uv}\frac{\overline{v^2} - 2\overline{u^2}}{\eta^+ + \delta Re}\right.$$
$$\left. - 3\overline{uv}\frac{\mathrm{d}\overline{u^2}}{\mathrm{d}\eta^+} - 6\overline{uv}\frac{\overline{u^2}}{\eta^+ + \delta Re}\right] - \frac{4\overline{uv}}{(\eta^+ + \delta Re)^2} - \overline{v^2}\frac{\mathrm{d}U^+}{\mathrm{d}\eta^+}$$
$$+ \overline{u^2}\frac{U^+}{\eta^+ + \delta Re} - (\overline{v^2} - \overline{u^2})\frac{U^+}{\eta^+ + \delta Re} - C_1(1 - f_{w,1})\frac{\epsilon}{k}\overline{uv}$$
$$+ (\alpha - \alpha^* f_{w,1})\left[\overline{v^2}\frac{\mathrm{d}U^+}{\mathrm{d}\eta^+} - \overline{u^2}\frac{U^+}{\eta^+ + \delta Re}\right]$$
$$- \beta\left[\overline{v^2}\frac{U^+}{\eta^+ + \delta Re} - \overline{u^2}\frac{\mathrm{d}U^+}{\mathrm{d}\eta^+}\right] - \gamma k\left[\frac{\mathrm{d}U^+}{\mathrm{d}\eta^+} - \frac{U^+}{\eta^+ + \delta Re}\right]$$
$$- f_{w,1}\frac{\epsilon}{k}\overline{uv} - 2f_{w,1}\frac{(\epsilon/k)\,\overline{uv}}{1 + 3\overline{v^2}/2k} = 0 \tag{12}$$

$$\frac{1}{\eta^+ + \delta Re}\frac{\mathrm{d}}{\mathrm{d}\eta^+}\left[(\eta^+ + \delta Re)\left(1 + C_\epsilon\frac{k}{\epsilon}\overline{v^2}\right)\frac{\mathrm{d}\epsilon}{\mathrm{d}\eta^+}\right]$$
$$+ C_{\epsilon 1}\frac{\epsilon}{k}(1 + \sigma f_{w,2})\left[-\overline{uv}\frac{\mathrm{d}U^+}{\mathrm{d}y^+} + \overline{uv}\frac{U^+}{\eta^+ + \delta Re}\right]$$
$$- C_{\epsilon 2}f_\epsilon\frac{\epsilon\tilde{\epsilon}}{k} + f_{w,2}\left[\left(\frac{7}{9}C_{\epsilon 2} - 2\right)\frac{\epsilon\tilde{\epsilon}}{k} - \frac{\epsilon^{*2}}{2k}\right] = 0 \tag{13}$$

where $\delta = r_c/h$ has been substituted. The boundary conditions are no slip for U^+, $\overline{u^2}$, $\overline{v^2}$, $\overline{w^2}$, and $\overline{uv}$ at $\eta^+ = -Re$ (convex wall) and $\eta^+ = Re$ (concave wall), and $2(\mathrm{d}\sqrt{k}/\mathrm{d}\eta^+)^2$ for ϵ at both the concave and convex walls.

VI. Discussion of Results

The governing equations are ordinary differential equations and can be easily solved using a Newton iteration scheme similar to the one used in Ref. 24. To resolve the near-wall flow correctly, fine grids have to be specified near the wall. A 61 point nonuniform grid with at least five grid points specified in the region $|Re| < \eta^+ < |Re| + 5$ and 15 grid points in the region $|Re| + 5 < \eta^+ < |Re| + 65$ is used to carry out the calculations. Convergence of the calculations is determined by an overall residual value of 10^{-5} or less.

The near-wall turbulence closure is formulated using the direct simulation data to shed light on the physics of near-wall

flows over curved surfaces. None of the calculated turbulence statistics have been used to calibrate the model constants. If the closure is to asymptote correctly to the high-Reynolds-number closure of Launder et al.,[14] which can predict curvature effects quite well outside of the near-wall region, then the model constants C_s, C_1, C_2, C_ϵ, $C_{\epsilon 1}$, and $C_{\epsilon 2}$ should take on the conventional values of 0.11, 1.5, 0.4, 0.15, 1.35, and 1.8, respectively. As for the constant α^*, Lai and So[19,25] found that a value of 0.45 gives the best overall prediction of pipe flow turbulence and heat transfer. The present objective is not to calibrate any of the model constants to achieve optimum agreement between closure calculations and a particular set of curved-flow data. Rather, the objective is to evaluate the physical arguments used to devise the closure and the general applicability of the closure for curved shear flows. Therefore, it is not advisable to vary the accepted values of the model constants. In view of this, the same set of model constants is used for the present calculations.

The near-wall turbulence closure with the model constants thus specified is used to calculate fully developed turbulent curved channel flows. Comparisons are made with direct simulation data[13] and measurements.[26] These two cases are selected for their widely different curvature parameter δ^{-1} and Reynolds number Re. For example, $\delta^{-1}=0.0127$ and $Re=168$ ($R_D=2990$) for the direct simulation data, while $\delta^{-1}=0.005$ and $Re=1330$ ($R_D=30{,}000$) for the measurements. This way, the Reynolds-number dependence of σ could also be tested. In the following comparisons, the turbulent flow properties presented are normalized by u_τ, except in the near-wall region (shown in the inset of each figure) where they are made dimensionless by the local friction velocity; i.e., by either $u_{\tau i}$ or $u_{\tau o}$, depending on whether the flow near the convex or the concave wall is examined. Furthermore, the local wall coordinate is taken to be given by $y^+=yu_{\tau i}/\nu$, where y is measured positive away from the wall, instead of by η^+. Therefore, once η^+ is known, y^+ can be calculated using the specified u_τ and the calculated $u_{\tau i}$ and $u_{\tau o}$. The mean velocities are normalized by the local friction velocity. This way of presenting the results is in accordance with that of Ref. 13 and will properly show the effects of curvature in the near-wall flow.

The comparisons with direct simulation data, with the contributions of the Taylor-Görtler vortices included, are shown in Figs. 2-4. It can be seen that the near-wall flow is correctly predicted by the proposed turbulence closure. For $y^+<20$, the predictions of U^+, $\overline{u^2}$, $\overline{v^2}$, and $\overline{w^2}$ are essentially identical to the direct simulation data (Figs. 2 and 3). In addition, there is no difference between the flow properties on the convex and concave walls. These results are consistent with the findings of Moser and Moin[13]; namely, the effects of curvature on U^+, $\overline{u^2}$, $\overline{v^2}$, and $\overline{w^2}$ in the near-wall region can be correctly accounted for by normalizing these quantities by local variables. In other words, there are two local velocity scales for curved channel flows and terms in the turbulent kinetic energy equation are not very sensitive to streamline curvature. These properties have been captured by the proposed near-wall turbulence closure.

On the other hand, terms in the Reynolds shear stress equation are very much affected by curvature. This leads to a separation of $\overline{uv}$ between the concave and convex wall values in the near-wall region, even when normalized by local variables (Fig. 4). The predictions of $\overline{uv}$ replicate this behavior quite well and lend credence to the near-wall turbulence closure proposed for curved flows. A further verification that the closure is appropriate for curved flows comes from the prediction of the ratio of wall friction velocity. In the calculation of this curved channel flow, Re or the global wall friction velocity is specified. Therefore, the accuracy in which the closure can predict the convex and concave wall friction velocities is a measure of the validity of the closure. The direct simulation data gives a value of 1.161 for the wall-friction velocity ratio and $u_{\tau o}/u_\tau=1.071$ and $u_{\tau i}/u_\tau=0.923$. These compare with predicted values of 1.101, 1.044, and 0.948, respectively. The

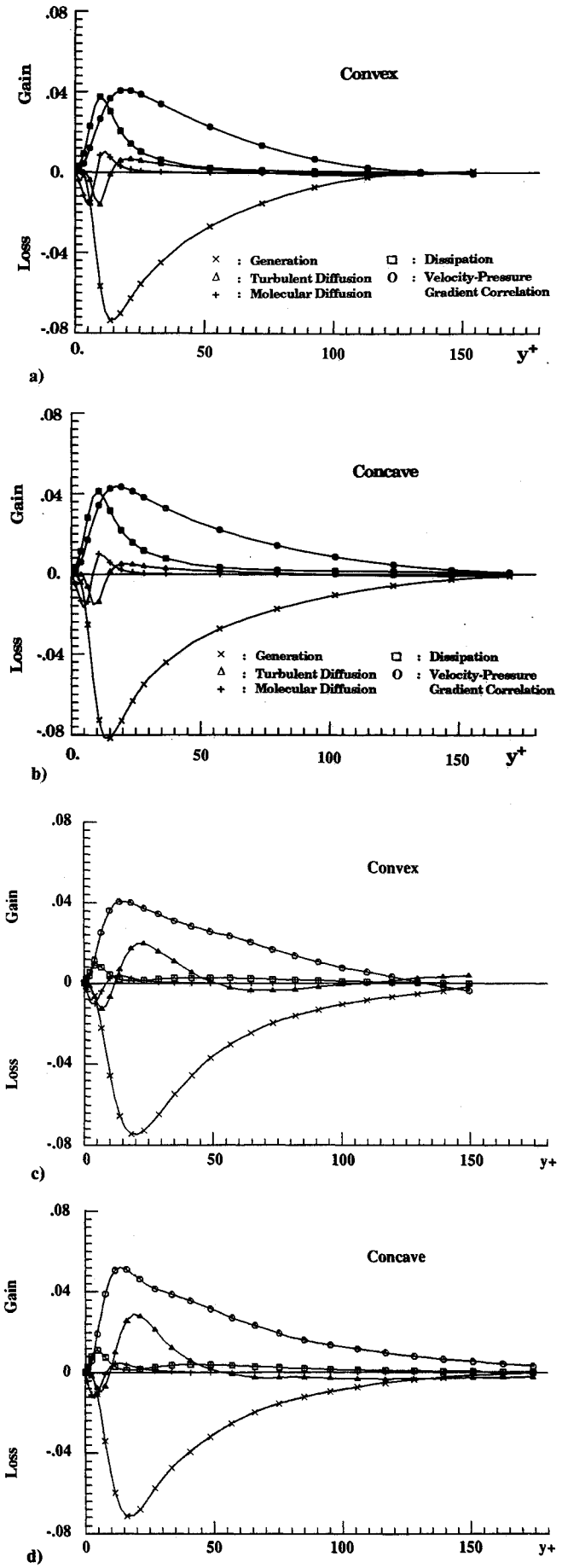

Fig. 7 Budgets of $\overline{uv}$ in the near-wall region. Model calculations: a) convex wall, and b) concave wall. Direct simulation: c) convex wall, and d) concave wall.

predicted wall friction velocity is lower on the concave wall and higher on the convex wall. However, the error is no more than 3 percent for each wall. In view of this fairly accurate prediction, the near-wall Reynolds stress closure can be said to be quite valid for curved channel flows.

The agreement between calculation and simulation data is less satisfactory in the region far away from the walls; in particular, those of $\overline{v^2}$ and the mean U^+ on the side of the convex wall (Figs. 2 and 3). The failing could be attributed to the high-Reynolds-number models used to approximate D_{ij}^T, Φ_{ij}, and ϵ_{ij} far away from the wall. In the regions where the discrepancies are most pronounced, $f_{w,1}$ and $f_{w,2}$ are close to zero and f_ϵ is about one. Therefore, the near-wall turbulence closure asymptotes to the high-Reynolds-number closure of Launder et al.[14] Since this closure is not formulated for flows with such a low overall Reynolds number ($R_D = 2990$), the agreement shown in Figs. 2–4 between calculation and simulation data is rather surprising. Therefore, it is believed that further improvements could be obtained by modifying the high-Reynolds-number models for D_{ij}^T, Φ_{ij}, and ϵ_{ij}, in addition to the present modifications for correct near-wall behavior.

Another reason for the discrepancy noted between model calculations and simulation data could be due to the presence of Taylor-Görtler vortices in the simulated curved channel flow and the lack of such in the model calculations. Moser and Moin[13] have shown that a pair of Taylor-Görtler vortices exist in the entire channel and are more concentrated on the concave side. This feature of curved channel flow has not been formulated into the model calculation. If the effect of the Taylor-Görtler vortices on the turbulence statistics is small, then the above comparisons would not be much influenced by these vortices. However, Moser and Moin[13] have demonstrated that the presence of the Taylor-Görtler vortices enhances the peaks of $\overline{u^2}$, $\overline{v^2}$, $\overline{w^2}$ and $\overline{uv}$ near the walls and contributes to an increase in $\overline{v^2}$ away from the wall on the concave side. In fact, the Taylor-Görtler vortices account for about half of the difference in Reynolds shear stress between the two sides of the channel in local wall variables and also $\sim 50\%$ of the difference between the wall shear stresses. Considering the fact that the model calculation ignores the contributions of the Taylor-Görtler vortices, the comparisons shown in Figs. 2–4 are quite good and the predicted wall shear stresses can be considered to be quite accurate. Therefore, the noted difference between simulation data and model calculations (Figs. 2–4) cannot be completely eliminated by improving the high-Reynolds-number models for D_{ij}^T, Φ_{ij}, and ϵ_{ij}. A formulation including the contributions of the Taylor-Görtler vortices is required. In other words, a three-dimensional formulation of the curved channel flow would be more appropriate. As for the turbulence closure, it is believed that the present model is more than adequate, even for a three-dimensional calculation of the curved channel flow.

The next set of comparisons is made with the budgets of the components of the Reynolds-stress equation. Only the budgets of $\overline{u^2}$, k, and $\overline{uv}$ are shown in Figs. 5–7. In these figures, a) shows the modeled budget near the convex wall, and b) that near the concave wall. Mansour et al.[17] have examined the high-Reynolds-number models for D_{ij}^T, Φ_{ij}, and ϵ_{ij} in a plane-channel flow and found that they are quite valid beyond $y^+ (= y\, u_\tau/\nu) > 100$, where y is measured positive away from the wall. The relations between y^+ and η^+ are given by $y^+ = -\eta^+ + Re$ for concave wall and $y^+ = \eta^+ + Re$ for convex wall. Furthermore, the budgets given by Moser and Moin[13] are limited to $y^+ < 100$. Therefore, the plots shown in Figs. 5–7 are for the range $0 \le y^+ \le 150$.

These calculations are in qualitative agreement with the simulation results. For example, the simulation budget data give a peak production of $\overline{u^2}$ at about $y^+ \cong 12$ and a peak value of about 0.45 near the concave wall and about 0.4 near the convex wall. The calculations also give a $y^+ \cong 12$ and approximately the same peak values near the concave and convex walls for the production of $\overline{u^2}$ (Fig. 5). The major discrepancy occurs in the predictions of ϵ_{ij}, all of which show a minimum away from the wall and finite values for ϵ_{uu} (Fig. 5), ϵ_{ww}, and ϵ (Fig. 6) and zero value for ϵ_{vv} at the wall. On the other hand, simulation results give a minimum at the wall for ϵ_{uu}, ϵ_{ww}, and ϵ and a zero for ϵ_{vv}. The minimum values calculated for ϵ_{uu}, ϵ_{ww}, and ϵ are about 2–3 times smaller than those given by direct simulation. In addition, the calculations of Φ_{ij}^* are not

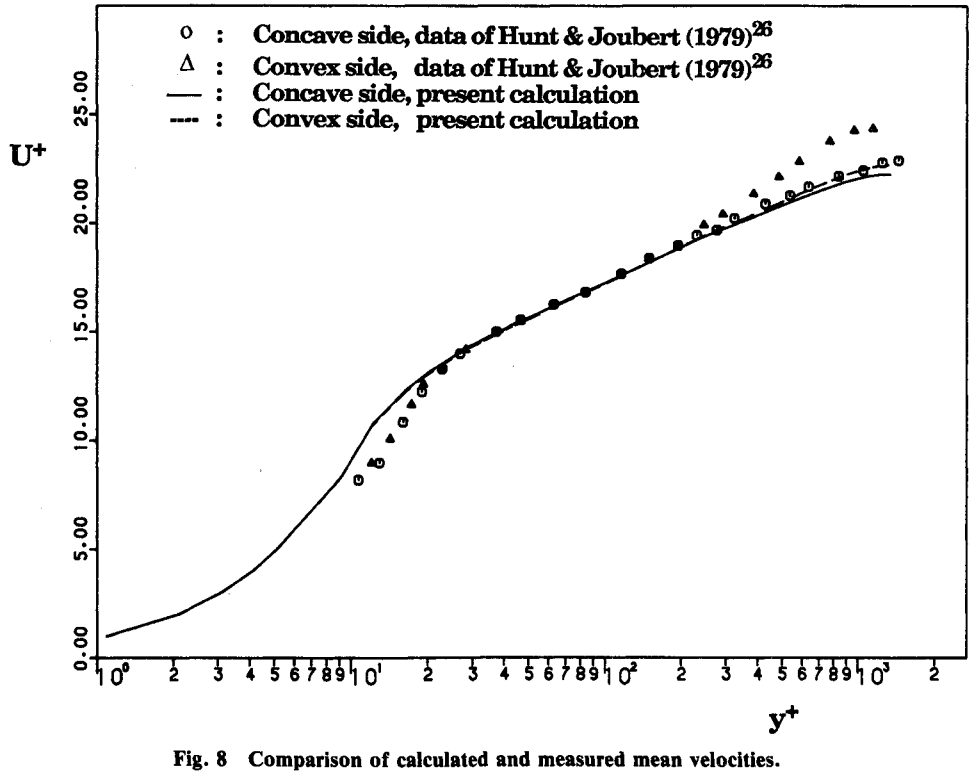

Fig. 8 Comparison of calculated and measured mean velocities.

quite correct quantitatively. However, in this case, the calculated minimum or maximum of Φ^*_{uu}, Φ^*_{ww}, Φ^*_{vv}, and Φ^*_{uv} are only about 1.1–1.5 times larger, while the calculated locations of the minimum and maximum are approximately correct for Φ^*_{uu}, Φ^*_{ww}, and Φ^*_{vv} and about twice as large as the simulation result for Φ^*_{uv}. Figures 5 and 7 show a minimum location for Φ^*_{uu} and a maximum location for Φ^*_{uv} at $y^+ \cong 15$. Contrast this with corresponding values of 25 and 15 from simulation results. These discrepancies could be traced to the inadequacy of the ϵ equation[19] and to the neglect of the contributions of the Taylor-Görtler vortices in the model calculations. In general, the proposed near-wall turbulence closure gives a reasonable prediction of the budgets of $\overline{u_i u_j}$ in the flow regions very close to the convex and concave walls. This is one characteristic that no other closures have yet been able to reproduce.

Another validation of the closure is carried out with the measurements of Hunt and Joubert.[26] In this experiment, the curvature parameter is about 2.5 times smaller and *Re* is approximately 10 times larger than the simulation data. Therefore, the data offers an opportunity to test the closure's ability

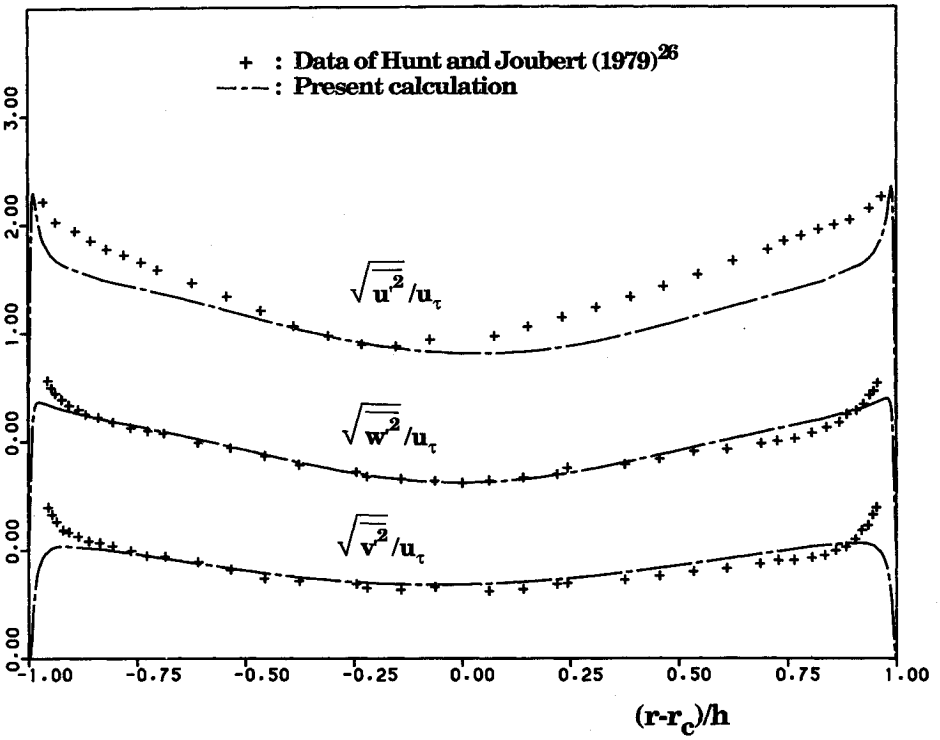

Fig. 9 Comparison of calculated and measured normal stresses.

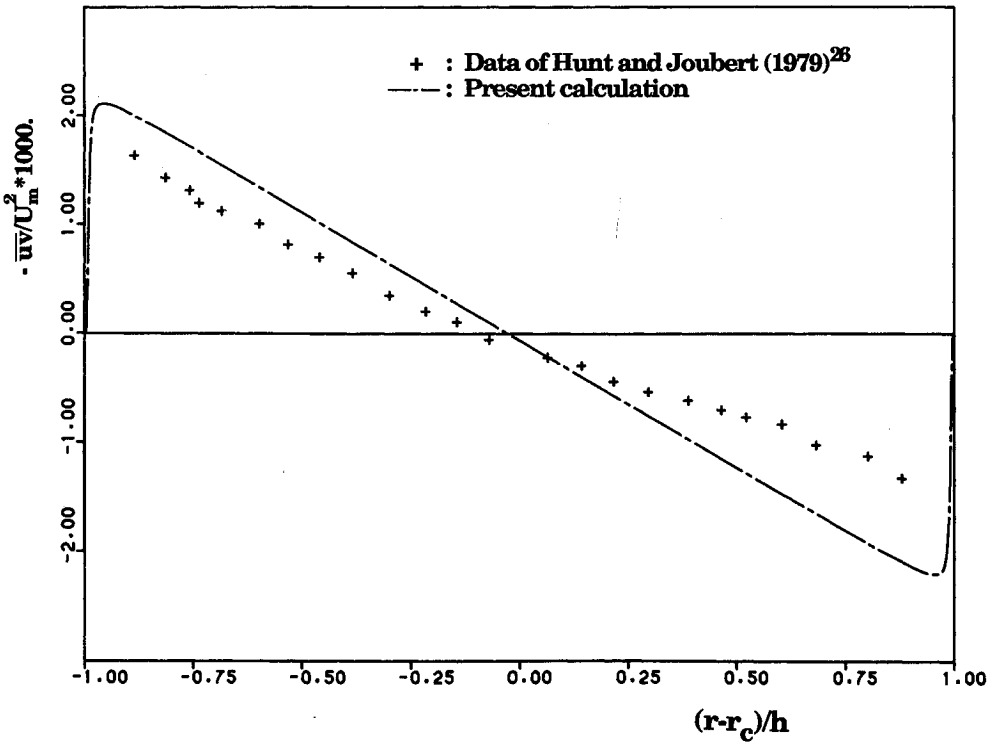

Fig. 10 Comparison of calculated and measured shear stresses.

to mimic the effects of Reynolds number, both in the near-wall and the fully turbulent flow regions. The comparisons are again made with the measured U^+, normal stresses and $\overline{uv}$, and are shown in Figs. 8–10. Good agreement is obtained for the mean velocities up to $y^+ \cong 250$ (Fig. 8). Beyond that, the calculated U^+ on the convex side is lower than the measurements. Again, the mean velocity on the convex and concave wall is identical in the region $0 < y^+ < 250$ when scaled by local variables. The discrepancy observed at large value of y^+ is similar to that noticed by So and Yoo[24] in their comparison with fully developed turbulent pipe flow data. They attributed the discrepancy to an inconsistency between the measured U^+ and $\overline{uv}$, because when these measured values are substituted into the mean momentum equation a slight imbalance resulted.

The agreement between the calculated and measured $\overline{v^2}$ and $\overline{w^2}$ is very good except in the regions near the convex and concave walls (Fig. 9). This result essentially verifies the validity of the high-Reynolds-number models for D_{ij}^T, Φ_{ij}, and ϵ_{ij} and supports the argument used to partially explain the discrepancy shown in Fig. 3 between calculated and simulated $\overline{v^2}$. The measurements of $\overline{v^2}$ and $\overline{w^2}$ show remarkable isotropy near the walls and a rather steep rise as the wall is approached. This behavior is contrary to that shown by plane channel flow measurements.[15] Since Hunt and Joubert[26] did not correct their cross-wire measurements for wall proximity effects, the measured $\overline{v^2}$ and $\overline{w^2}$ could be in error near the wall. In addition, their wire length is about 42 (ν/u_τ), which is more than twice the tolerable limit found by Ligrani and Bradshaw[27] for accurate near-wall measurements.

On the other hand, the agreement for $\overline{u^2}$ is poor, in particular, on the side of the concave wall. The reason could be due to the concentration of Taylor-Görtler type vortices on the concave wall. In the experiment, these vortices were found to penetrate all the way to the channel mean radius.[26] Since the measurements were carried out along the channel midplane, it is not clear whether this location corresponds to the up-swell or to the down-swell of the vortices. According to boundary-layer measurements on a concave wall[28] $\overline{u^2}$ measured at these two locations differ significantly. This could also explain the poor agreement shown for $\overline{uv}$ on the side of the concave wall because the curved channel measurements show a significant $\overline{uw}$ near the concave wall and are consistent with the measurements of Ref. 28.

The preceding analysis shows the difficulty of two-dimensional turbulent flow modeling over concave surfaces, especially when Taylor-Görtler type vortices are present in the flow. As demonstrated by the measurements of Hunt and Joubert,[26] these vortices are present even for a curvature parameter as small as 0.005. When Taylor-Görtler type vortices are present, the mean flow is hardly two-dimensional[28] and the vortices are found to have significant impact on the turbulence statistics.[13]

VII. Conclusions

A near-wall Reynolds-stress closure for curved shear flows has been formulated. Insight gained by examining the direct simulation data of a curved channel flow, in particular, the near-wall flow behavior at the convex and concave walls is used to devise modifications to conventional high-Reynolds-number models for the pressure-strain term and the viscous-dissipation function near a wall. The resultant models are required to satisfy the near-wall behavior of the terms they replaced and to give rise to a modeled Reynolds-stress equation with terms that remain in balance as the wall is approached. In addition, the variables have to satisfy the no-slip condition at the wall. Thus modeled, the Reynolds-stress equation is valid over the whole field and can be solved without invoking the wall-function assumptions. The closure also has the unique advantage of asymptotically approaching the high-Reynolds-number closure of Launder et al.[14] far away from the wall. Therefore, streamline curvature effects in this region are also properly modeled.

The near-wall turbulence closure is validated against the low-Reynolds-number simulation data of Moser and Moin[13] and the high-Reynolds-number measurements of Hunt and Joubert.[26] The closure is capable of reproducing the major findings of Moser and Moin in a curved channel flow. These are 1) the similarity of U^+, $\overline{u^2}$, $\overline{v^2}$, and $\overline{w^2}$ at the convex and concave walls when scaled by local variables; 2) the separation of $\overline{uv}$ between the concave and convex wall values in the near-wall region, even when they are scaled by local variables; and 3) the importance of modeling the pressure-strain term to account for curvature effects. The predicted U^+, $\overline{u^2}$, $\overline{v^2}$, $\overline{w^2}$, and $\overline{uv}$ are in good agreement with both simulation data and measurements, even though the Reynolds numbers of the two cases differ by a factor of ten. This shows that the proposed closure is applicable for a rather wide range of Reynolds number.

Acknowledgment

This work was partially supported by the David Taylor Research Center, Annapolis, Maryland under Contract N00167-86-K-0075 and partially by NASA Langley Research Center, Hampton, Virginia under Grant NAG-1-1080.

References

[1]Bradshaw, P., "The Analogy Between Streamline Curvature and Buoyancy in Turbulent Shear Flow," *Journal of Fluid Mechanics*, Vol. 36, 1969, pp. 177–191.

[2]So, R. M. C., "A Turbulent Velocity Scale for Curved Shear Flows," *Journal of Fluid Mechanics*, Vol. 70, 1975, pp. 37–57.

[3]So, R. M. C., and Mellor, G. L., "Turbulent Boundary Layers with Large Streamline Curvature Effects," *Zeitschrift für Angewandte Mathematik und Physik*, Vol. 32, 1981, pp. 514–532.

[4]So, R. M. C., "Heat-Transfer Modeling for Turbulent Shear Flows on Curved Surfaces," *Zeitschrift für Angewandte Mathematik und Physik*, Vol. 32, 1981, pp. 514–532.

[5]Lischziner, M. A., and Rodi, W., "Calculation of Annular and Twin Parallel Jets Using Various Discretization Schemes and Turbulence—Model Variations," *Journal of Fluids Engineering*, Vol. 103, 1981, pp. 352–360.

[6]Gibson, M. M., "An Algebraic Stress and Heat-Flux Model for Turbulent Shear Flow with Streamline Curvature," *International Journal of Heat and Mass Transfer*, Vol. 21, 1978, pp. 1609–1617.

[7]Wilcox, D. L., and Chambers, T. L., "Streamline Curvature Effects on Turbulent Boundary Layers," *AIAA Journal*, Vol. 15, 1977, pp. 574–580.

[8]Irwin, H. P. A. H., and Arnot Smith, P., "Prediction of the Effects of Streamline Curvature on Turbulence," *The Physics of Fluids*, Vol. 18, 1975, pp. 624–630.

[9]Gibson, M. M., Jones, W. P., and Younis, B. A., "Calculation of Turbulent Boundary Layers on Curved Surfaces," *The Physics of Fluids*, Vol. 24, 1981, pp. 386–395.

[10]So, R. M. C., and Mellor, G. L., "Experiment on Convex Curvature Effects in Turbulent Boundary Layers on Curved Surfaces," *Journal of Fluid Mechanics*, Vol. 60, 1973, pp. 43–62.

[11]Kline, S. J., Cantwell, B. J., and Lilley, G. M. (eds.), *Proceeding of the 1980–1981 AFOSR—HTTM—Stanford Conference on Complex Turbulent Flows*, Vol. 1, Dept. of Mechanical Engineering, Stanford Univ., Stanford, CA 94035.

[12]Bradshaw, P., "The Effects of Streamline Curvature on Turbulent Flow," AGARDograph 169, 1973.

[13]Moser, R. D., and Moin, P., "The Effects of Curvature in Wall-Bounded Turbulent Flow," *Journal of Fluid Mechanics*, Vol. 175, 1987, pp. 479–510.

[14]Launder, B. C., Reece, G. J., and Rodi, W., "Progress in the Development of a Reynolds-Stress Turbulence Closure," *Journal of Fluid Mechanics*, Vol. 68, 1975, pp. 537–566.

[15]Kreplin, H., and Eckelmann, H., "Behavior of the Three Fluctuating Velocity Components in the Wall Region of a Turbulent Channel Flow," *The Physics of Fluids*, Vol. 22, 1979, pp. 1233–1239.

[16]Kim, J., Moin, P., and Moser, R. D., "Turbulence Statistics in Fully Developed Channel Flow at Low Reynolds Number," *Journal of Fluid Mechanics*, Vol. 177, 1987, pp. 133–186.

[17]Mansour, N. N., Kim, J., and Moin, P., "Reynolds-Stress and Dissipation-Rate Budgets in a Turbulent Channel Flow," *Journal of Fluid Mechanics*, Vol. 192, 1988, pp. 15–44.

[18]Hanjalic, K., and Launder, B. E., "A Reynolds-Stress Model of

Turbulence and Its Application to Thin Shear Flows," *Journal of Fluid Mechanics*, Vol. 52, 1972, pp. 609–638.

[19]Lai, Y. G., and So, R. M. C., "On Near-Wall Turbulent Flow Modeling," *Journal of Fluid Mechanics*, Vol. 221, 1990, pp. 641–673.

[20]Kolmogorov, A. N., "Local Structure of Turbulence in Incompressible Viscous Fluid for Very Large Reynolds Number," *Doklady AN SSSR*, Vol. 30, 1941, pp. 299–303.

[21]Launder, B. E., and Reynolds, W. C., "Asymptotic Near-Wall Stress Dissipation Rates in a Turbulent Flow," *The Physics of Fluids*, Vol. 26, 1983, pp. 1157–1158.

[22]Shima, N., "A Reynolds-Stress Model for Near-Wall and Low-Reynolds-Number Regions," *Journal of Fluids Engineering*, Vol. 110, 1988, pp. 38–44.

[23]Mansour, N. N., Kim, J., and Moin, P., "Wall k–ϵ Turbulence Modeling," *AIAA Journal*, Vol. 27, 1989, pp. 1068–1073.

[24]So, R. M. C., and Yoo, G. J., "Low-Reynolds-Number Modeling of Turbulent Flows with and without Wall Transpiration," *AIAA Journal*, Vol. 25, 1987, pp. 1556–1564.

[25]Lai, Y. G., and So, R. M. C., "Near-Wall Modeling of Turbulent Heat Fluxes," *International Journal of Heat and Transfer*, Vol. 33, 1990, pp. 1429–1440.

[26]Hunt, I. A., and Joubert, P. N., "Effects of Small Streamline Curvature on Turbulent Duct Flow," *Journal of Fluid Mechanics*, Vol. 91, 1979, pp. 633–659.

[27]Ligrani, P. M., and Bradshaw, P., "Spatial Resolution and Measurement of Turbulence in the Viscous Sublayer Using Subminiature Hot-Wire Probes," *Experiments in Fluids*, Vol. 5, 1987, pp. 407–417.

[28]So, R. M. C., and Mellor G. L., "Experiment on Turbulent Boundary Layer on a Concave Wall," *Aeronautical Quarterly*, Vol. 26, 1975, pp. 25–40.